11-28-2020

Improvement of light intensity and efficiency of n-ZnO/NiO/p-GaN heterojunction-based white light emitting diodes using micro-/nanolens array

Apurba Adhikary

Md Shamim Ahsan

Md Mahbub Hossain

Md Bipul Hossain

S. H. Shah Newaz

See next page for additional authors

Recommended Citation

Apurba Adhikary, Md. Shamim Ahsan, Md. Mahbub Hossain, Md. Bipul Hossain, S.H. Shah Newaz, Farid Ahmed, and Ik-Bu Sohn "Improvement of light intensity and efficiency of n-ZnO/NiO/p-GaN heterojunction-based white light emitting diodes using micro-/nanolens array," Optical Engineering 59(11), 117108 (28 November 2020). https://doi.org/10.1117/1.OE.59.11.117108

Improvement of light intensity and efficiency of n-ZnO/NiO/p-GaN heterojunction-based white light emitting diodes using micro-/nanolens array

Apurba Adhikary,[a,b] **Md. Shamim Ahsan**,[a,*] **Md. Mahbub Hossain**,[a] **Md. Bipul Hossain**,[b] **S.H. Shah Newaz**,[c,d] **Farid Ahmed**,[e] **and Ik-Bu Sohn**[f,*]

[a]Khulna University, Science Engineering and Technology School, Electronics and Communication Engineering Discipline, Khulna, Bangladesh

[b]Noakhali Science and Technology University, Department of Information and Communication Engineering, Noakhali, Bangladesh

[c]Universiti Teknology Brunei, School of Computing and Informatics, Gadong, Brunei Darussalam

[d]Korea Advanced Institute of Science and Technology, KAIST Institute for Information Technology Convergence, Daejeon, Republic of Korea

[e]University of Texas Rio Grande Valley, Manufacturing and Industrial Engineering, Edinburg, Texas, United States

[f]Gwangju Institute of Science and Technology, Advanced Photonics Research Institute, Gwangju, Republic of Korea

Abstract. Our study proposes a technique to enhance light extraction efficiency of light emitting diodes (LEDs) by incorporating various micro-/nanolens arrays (MNLAs) on the substrate layer, which in turn increases the external quantum efficiency (EQE) of the LEDs. To simulate the LEDs, we utilized the finite difference time domain method. To achieve a white LED, we inserted a thin layer of NiO at the interface between the n-type ZnO and the p-type GaN. The basic n-ZnO/NiO/p-GaN heterojunction-based LED exhibited an EQE of 10.99% where the effective refractive index of the LED structure was 1.48. The EQE was further increased by engraving various planoconvex or planoconcave MNLA on the top surface of the substrate layer. A maximum EQE of 12.4% was achieved for convex-1 type (lens height of 0.5 μm and radius of 0.4 μm) elliptical lens engraved LED where the effective refractive index was 1.4. In addition, the peak electroluminescence (EL) light intensity of convex-1 lens-based LED was twice than the light intensity observed in basic LED. Because of excellent EL spectrum and significant amount of light throughout the visible spectrum, the proposed convex-1 structure-based LED can be considered as a prospective candidate for white LED. © *2020 Society of Photo-Optical Instrumentation Engineers (SPIE)* [DOI: 10.1117/1.OE.59.11.117108]

Keywords: light emitting diode; micro-/nanostructuring; light extraction efficiency; electroluminescence intensity; finite difference time domain.

Paper 20200784 received Jun. 30, 2020; accepted for publication Nov. 12, 2020; published online Nov. 28, 2020.

1 Introduction

The light-emitting diode is a key component in today's lighting technology. The unique properties of LEDs such as compactness, low-power consumption, long lifetime, and fast turn-on time have made these devices an indispensable part of modern traffic lighting, display, car lighting, and cell phone technologies.[1] An LED is an electroluminescent device with a broad selection of emission wavelengths and emits light when an electric current passes through it. Most of the LEDs are monochromatic, i.e., emit light at a single wavelength. The output from an LED can range from red (wavelength varies around 700 nm) to blue-violet (about 400 nm). Some LEDs emit energy in the infrared region (830 nm or longer), those are known as infrared-emitting

*Address all correspondence to Md. Shamim Ahsan, shamim@kaist.ac.kr: Ik-Bu Sohn ibson@gist.ac.kr

diodes. Blue LEDs emit energy in the wavelength range of 450 to 495 nm, whereas green LEDs emit energy in the wavelength range between 495 to 570 nm.[2] An LED consists of two fundamental elements of processed materials namely, p-type semiconductors and n-type semiconductors. These two elements are placed in direct contact to form the p–n junction. The key difference of an LED from the conventional p–n junction is its transparent packaging that allows radiation of visible energy through it.[3]

Considerable research has been devoted to the development and fabrication of red LEDs,[4,5] green LEDs,[6,7] blue LEDs,[8,9] and white LEDs.[10,11] Hwang et al.[4] reported the fabrication of an InGaN-based red LED operating at the wavelength of 629 nm with an external quantum efficiency (EQE) of 2.9% and a light output power of 1.1 mW at 20 mA. An InGaInP epilayer-based red-light micro-LED display was proposed by another research group.[5] The demonstrated micro-red LED features a maximum output power of 4.45 mW with a brightness of 464 nits at the driving current of 48 mA. EQE up to 4.2% was reported in that study at the driving current of 30 mA. A low-intensity green LED, operating at 532 nm, was reported for curing acrylate-based dental resins that emits light with intensities of 6 to 10 mW/cm^2.[6] Vashishtha et al.[7] constructed a high-intensity green LED using Ruddlesden–Popper inorganic mixed halide perovskites with butylammonium interlayers. Their findings impart that a maximum EQE of 10.1% was achieved for a current density of 16.3 mA/cm^2. Liu et al.[8] utilized quantum-confined bromide perovskite nanostructures to demonstrate an efficient blue LED, operating at 483 nm. An EQE up to 9.5% was achieved at a luminance of 54 cd/m^2 with excitation density as low as 0.3 mW/cm^2. Spectra stable perovskite blue LED, operating in a wide spectral region (454 to 592 nm), was also reported where a peak EQE of 1.35% with a minimum excitation density of 1.5 mW/cm^2 and peak luminance of 100.6 cd/m^2 was achieved.[9] Several studies have investigated how white light emission can be achieved through hybridizing the blue emission of GaN with deep-level emission of ZnO.[10,11] Nguyen et al.[10] proposed a technique of building white LED by coating a solution of phosphor ($Y_3A_{15}O_{12}:Ce$) on GaN-based blue LED chips having an emission wavelength of 450 nm. The power of the fabricated white LED was 40 lm/W. Chen et al.[11] transformed a GaN-based blue LED to a white LED by utilizing 10% to 40% cerium doped yttrium aluminum garnet phosphor ($YAG:Ce^{3+}$) incorporated flexible polydimethylsiloxane (PDMS) substrate. The proposed PDMS substrate revealed the 470-nm peak of the blue LED.

Most of the current LED-based research works are focused on improving the optical, thermal, and energy performance of the LEDs. The two key important ways of performance enhancement of LEDs are increasing the output light intensity and light extraction efficiency. Proper selection of materials in each layer of the LEDs and refractive index matching among the adjacent layers lead to higher efficiency LED. In order to increase the light intensity and light extraction efficiency of LEDs, improvements of the external and internal quantum efficiency (IQE) of the LEDs are required. The IQE is the fraction of the electron–hole pairs that recombine radiatively in the active region. On the contrary, EQE is defined as the ratio of the photons emitted from the LED to the number of internally generated photons. However, increasing the external and IQE of LEDs using the conventional technologies are very much challenging. The IQE of an LED can be improved by changing the materials of different layers and appropriate matching of refractive indices of different layers. In contrast, the EQE can be enhanced by micro-/nanostructuring layers of the LEDs. The out-coupling efficiency as well as EQE of the LEDs can be improved by optimizing the physical parameters of the micro-/nanometric structures. Abbasi et al.[12] proposed enhancement of light emission from white LED by means of n-ZnO/NiO/p-GaN heterojunction structure where they deposited NiO buffer layer on top of GaN substrate. To achieve high-efficiency white LED, the researchers grown different morphologies of ZnO nanorods and nanotubes on top of the NiO layer. Until now, the research works focused on micro-/nanostructures-based enhancement of EQE of LEDs are limited. However, various micro-/nanometric structures were proven beneficial in designing various photonic devices and predicted to have great potential in enhancing the light intensity and EQE of LEDs.[13–16] Therefore, more investigations are required to optimize the micro-/nanometric structures for LEDs.

In this work, we introduce a mechanism for improving light extraction efficiency of white LEDs. We have considered n-ZnO/NiO/p-GaN type white LED because of their excellent light confinement due to the impeding of electron injections from the ZnO to the GaN by a thin NiO

layer. We attain high-electroluminescence (EL) light intensity and EQE by incorporating a large variety of planoconvex and planoconcave lens array at the end face of the substrate layer. The performance of our designed LEDs has been evaluated by means of FDTD method. The results obtained from FDTD method impart that, in our solution the EQE can reach up to 12.4% by engraving convex-1 type elliptical micro-/nanolens array (MNLA), with lens height of 0.5 μm and lens radius of 0.4 μm, on the substrate layer of a white LED. Compared to basic white LED, significant improvement of EL intensity of light (enhanced from 9760 to 20,000 a.u.) is also obvious in the convex-1 type MNLA-based white LED. Furthermore, convex-1 type LED has shown substantial light intensity throughout the visible spectrum that confirms the formation of white LED. Moreover, excellent light distribution is evident for convex-1 type MNLA-based white LED. The authors believe that the proposed efficiency improvement technique will pave the way for fabricating highly efficient LEDs.

2 Fundamental Concepts of Light Emitting Diode

An LED is a p–n junction, where p-type and n-type semiconductor materials are in contact with each other. When a forward electric current or voltage is applied at the p–n junction, electrons meet the holes and fall into a lower energy level. As a result, energy is released in the form of photons and a narrow bandwidth visible or invisible light is emitted.[17] The most popular way of achieving white LEDs is the insertion of NiO layer in between the p-type GaN and n-type ZnO. Among all kinds of recombination, only radiative recombination rate determines the efficiency of LEDs. The efficiency of an LED is dependent on both the internal and EQE. The IQE (η_{int}) of an LED can be determined as follows:[17]

$$\eta_{\text{int}} = \frac{1}{1 + (\tau_R/\tau_{\text{NR}})} = \frac{\tau}{\tau_R}, \tag{1}$$

where τ_R is the radiative recombination time, τ_{NR} is the non-radiative recombination time, and the bulk recombination lifetime τ can be defined by $1/\tau = 1/\tau_R + 1/\tau_{\text{NR}}$. The radiative and non-radiative recombination times are limited to materials' properties. On the contrary, EQE (η_{ext}) of an LED can be defined as follows:[18]

$$\eta_{\text{ext}} = \frac{\phi}{I} = \frac{P\lambda}{Ich}, \tag{2}$$

where P is the emitted power of the LED, λ is the wavelength of the emitted light, c is the speed of light, I is the injected current, and h is the Plank's constant. EQE is dependent on the injection current. The EQE can also be estimated using the following equation:[19]

$$\eta_{\text{ext}} = \frac{1}{n_e(n_e + 1)^2}, \tag{3}$$

where n_e is the effective refractive index of the LED structure.

3 Materials and Methods

3.1 *Material Properties*

We designed surface emitting white LEDs by varying the physical properties of the substrate layer. The proposed LED consists of the following layers: anode, cathode, hole-transport layer (HTL), active layer/recombination layer, electron-transport layer (ETL), and substrate. We considered nickel (Ni) as anode and aluminum (Al) as cathode. As a HTL, we incorporated p-type gallium nitride (GaN) in our proposed LEDs. In contrast, n-type zinc oxide (ZnO) was utilized as the ETL. In our LEDs, we used highly transparent silicon dioxide (SiO_2) as the substrate. To increase the light extraction efficiency of our proposed LEDs, wide varieties of micro-/nanostructures were engraved on the outer surface of the substrate layer. To convert electric

Table 1 Physical parameters of different layers of the designed LEDs.[20]

Layer name	Length (μm)	Thickness (μm)	Refractive index	Lattice constant (Å)	Material
Cathode	4	0.20	1.36 at 650 nm	4.046	Al
Anode	2	0.20	2.04 at 650 nm	3.499	Ni
Hole-transport layer	8	1.00	2.18 at 650 nm	$a = 3.189$ $c = 5.186$	p-GaN
Electron-transport layer	8	0.60	1.997 at 650 nm	4.580	n-ZnO
Active layer	8	0.20	2.26	4.177	NiO
Substrate	2	0.40	1.45 at 650 nm	$a = 4.914$ $c = 5.405$	SiO_2

energy to light, a thin layer of nickel oxide (NiO) was sandwiched between the n-type Zno and p-type GaN material as the active layer. As a result, light was emitted from the surface of the LEDs. The physical parameters of different layers of the designed LEDs are summarized in Table 1.

3.2 *Design Parameters of Our Proposed LEDs*

We started our research with a basic LED structure. The schematic diagram of a basic n-ZnO/NiO/p-GaN heterojunction LED without any micro-/nanometric structure on the substrate layer is illustrated in Fig. 1(a). After the incorporation of micro-/nanostructure on the substrate layer, the physical structure of the LED became like Fig. 1(b). Band diagrams of the n-ZnO/NiO/p-GaN junction are depicted in Fig. 1(c). The electron and hole barriers of n-type ZnO and p-type GaN are 0.15 and 0.12 eV, respectively. The energy barrier of holes and electrons at the interfaces of the ZnO/NiO and the NiO/GaN are 2.89 and 2.28 eV, respectively. The difference of the energy band offsets in the presence of NiO layer indicates blocking of transport of electrons

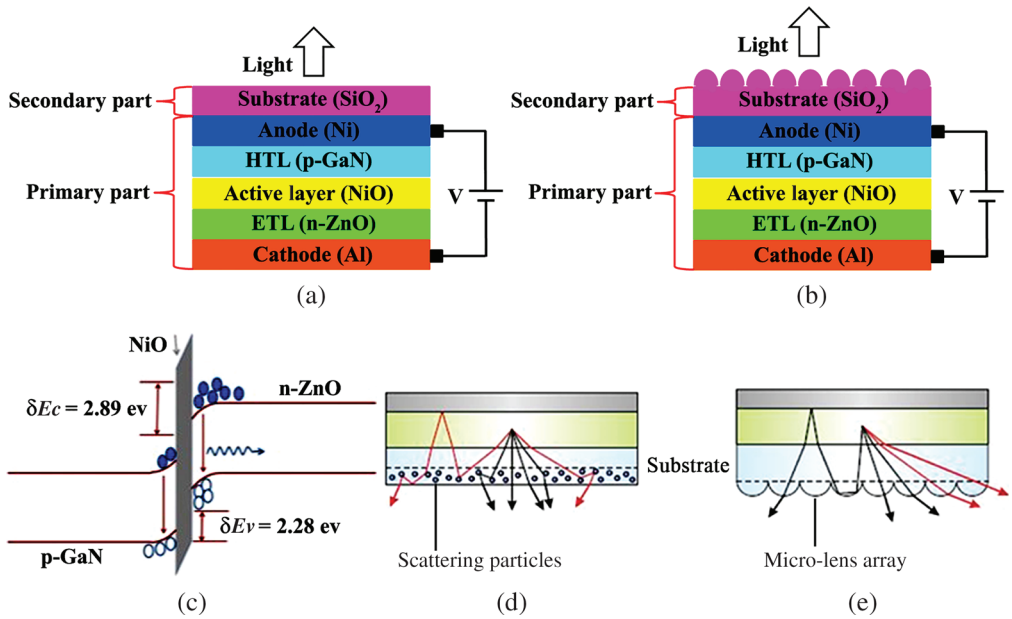

Fig. 1 (a) Schematic diagram of the basic n-ZnO/NiO/p-GaN heterojunction LED; (b) schematic diagram of the micro-structure engraved n-ZnO/NiO/p-GaN heterojunction LED; (c) band diagrams of the n-ZnO/NiO/p-GaN LED;[12] (d) trapping of light in the substrate layer due to TIR in the basic LED model of (a);[21] and (e) increase of light output-coupling efficiency by micro-/nanostructure incorporated LED of (b).[21]

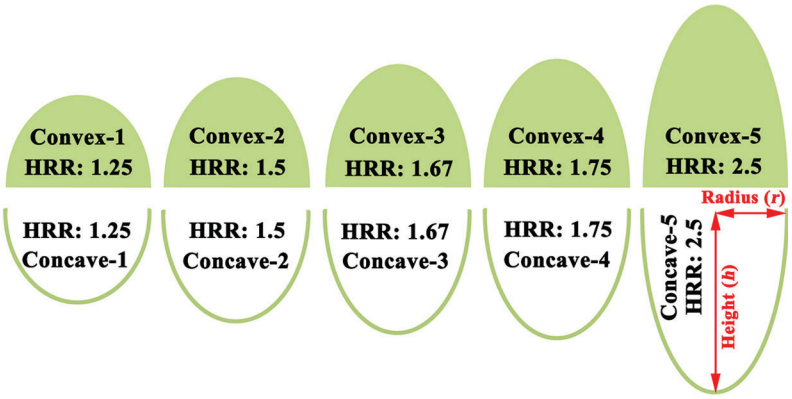

Fig. 2 The shape of various kinds of elliptical micro-/nanolenses engraved in the substrate layer of the LEDs.

from the ZnO layer to the GaN layer. For the flat substrate of the basic LED of Fig. 1(a), light is trapped inside the substrate layer because of TIR at the air/substrate interface, as shown in Fig. 1(d). The addition of microlens array [see Fig. 1(b)] can reduce the TIRs at the air/substrate interface, which in turn increases the out-coupling efficiency as well as overall efficiency of the microlens engraved LEDs, as illustrated in Fig. 1(e). The red-light paths in Figs. 1(d) and 1(e) indicate the light comes out from the LEDs that would normally be trapped inside the substrate due to TIR at the air/substrate interface. When the lenses were purely spherical, the value of the height and radius was the same. As a result, the height-to-radius ratio (HRR) of the spherical lenses was always 1. During our simulation, we utilized both planoconvex and planoconcave spherical lenses. In contrast, five different kinds of planoconvex lenses (convex-1 to convex-5) and planoconcave lenses (concave-1 to concave-5) were considered during the design of the LEDs, as shown in Fig. 2.

For the elliptical lenses, the major axis radius was considered as the height and minor axis radius was considered as the radius of the lenses. The HRR of the convex-1 and concave-1, convex-2 and concave-2, convex-3 and concave-3, convex-4 and concave-4, and convex-5 and concave-5 lenses was 1.25, 1.5, 1.67, 1.75, and 2.5, respectively. The radius of curvature (R) of the micro-/nanolenses can be estimated using the following equation:[22]

$$R = \frac{h^2 + r^2}{2\ h}, \tag{4}$$

where h and r represent the height and radius of the micro-/nanolens. The focal length (f) of the micro-/nanolenses is calculated using the following equation:[22]

$$f = \frac{R^2 + h^2}{2\ h(n-1)} - h(n-1), \tag{5}$$

where n is the refractive index of the micro-/nanolenses, i.e., substrate material ($n = 1.45$).

3.3 *Models of Various LEDs*

At first, we designed the basic n-ZnO/NiO/p-GaN heterojunction LED where micro-/nanometric structures were absent in the substrate layer. Figure 3(a) represents the two-dimensional (2D) layout of the basic model of n-ZnO/NiO/p-GaN heterojunction white LED. The 2D refractive index distribution of the basic model is illustrated in Fig. 3(d). To increase the light efficiency, we incorporated MNLA on the substrate layer. Both planoconvex and planoconcave MNLA of different sizes and shapes (spherical and elliptical) were considered during designing the LEDs. Fig. 3(b) shows the 2D layout of the LED having planoconvex elliptical lens engraved substrate, whereas the 2D refractive index distribution is illustrated in Fig. 3(e). The 2D layout and

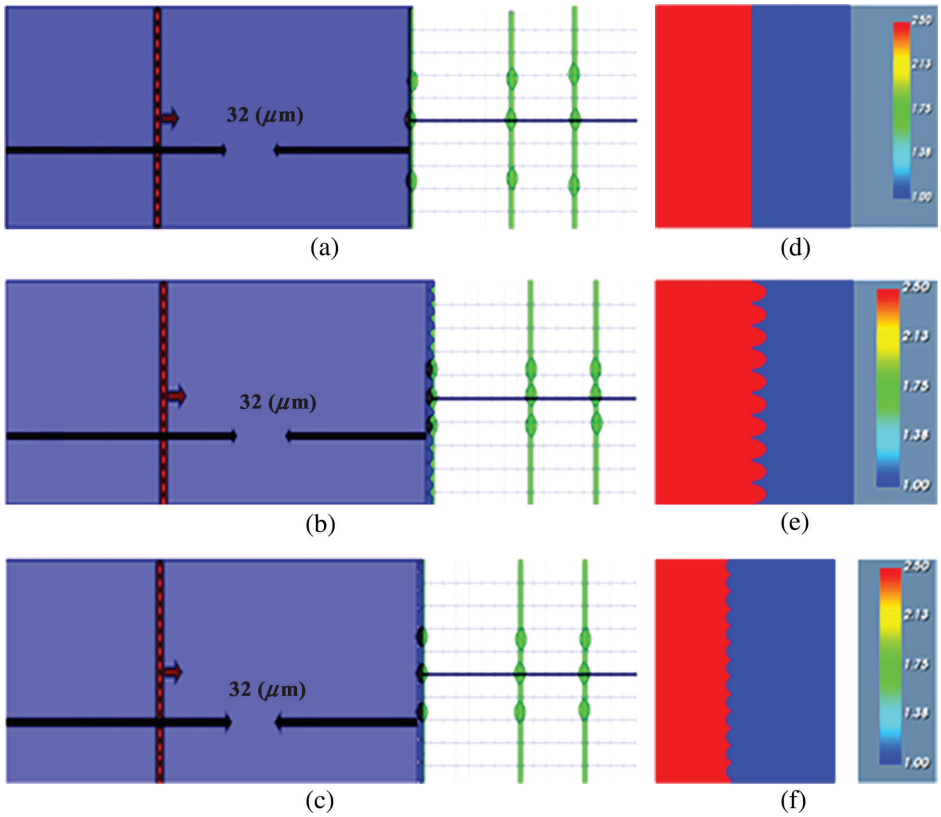

Fig. 3 (a)–(c) 2D layout and (d)–(f) refractive index distribution of various light emitting diodes designed using OptiFDTD simulator: (a), (d) basic model; (b), (e) planoconvex elliptical lens engraved model; and (c), (f) planoconcave spherical lens engraved model (SiO_2: red color and air: blue color).

refractive index distribution of the planoconcave spherical lens engraved LED is depicted in Figs. 3(c) and 3(f) where the periodic elliptical lenses are placed at the end face of the substrate. In this model, an array of half circles is placed at the end face of the substrate layer.

For spherical lenses, we varied the radius from 0.4 to 0.7 μm for both the planoconvex and planoconcave lenses, where the HRR of the spherical lenses was 1. For both kinds of elliptical lenses (planoconvex and planoconcave), there are two types of axis: major axis (lens height) and minor axis (lens radius). At first, we fixed the value of the lens height to 0.5 μm; the lens radius was varied from 0.2 to 0.4 μm. Afterarward, we kept the lens radius to 0.4 μm and the lens height was varied between 0.5 and 0.7 μm. The HRR value of the elliptical micro-/nanolenses was varied between 1.25 and 2.5. The physical parameters of the planoconvex and planoconcave spherical and elliptical lenses are summarized in Table 2.

3.4 *Simulation and Analysis*

We designed different kinds of white LED and simulated the models using commercial OptiFDTD [Version: 13.0 (64 bit)] simulator. Various optical properties such as EL spectrum and 2D and 3D image maps of discrete Fourier transform (DFT) of the electric field in the y direction (E_y) of the designed LEDs were investigated. We examined the EL spectrum of light from 0.35 to 0.9 μm. The simulations were carried out under room temperature (i.e., 25°C) where the simulations were run for 1000 time steps with mesh delta X (μm) of 0.05, mesh delta Y (μm) of 0.05, and mesh delta Z (μm) of 0.05. To analyze the simulation results, we considered three observation points from the end face of the substrate (near field: 0 μm, far field 1:8 μm, and far field 2:13 μm). We also investigated the effective refractive index of the basic LED structure and different MNLA incorporated LED structures.

Table 2 Physical parameters of the micro-/nanolenses engraved in the substrate of the LEDs.

Lens type	Lens height (h) and radius (r) (μm)	HRR	Radius of curvature (R) (μm)	Focal length (f) (μm)
Planoconvex micro-/nanolenses				
Spherical	0.4/0.5/0.6/0.7	1	0.4/0.5/0.6/0.7	0.71/0.89/1.06/1.24
Convex-1	h: 0.5; r: 0.4	1.25	0.41	0.7
Convex-2	h: 0.6; r: 0.4	1.5	0.43	0.74
Convex-3	h: 0.5; r: 0.3	1.67	0.34	0.59
Convex-4	h: 0.7; r: 0.4	1.75	0.46	0.8
Convex-5	h: 0.5; r: 0.2	2.5	0.29	0.52
Planoconcave micro-/nanolenses				
Spherical	0.4/0.5/0.6/0.7	1	−0.4/−0.5/−0.6/−0.7	−0.71/−0.89/−1.06/−1.24
Concave-1	h: 0.5; r: 0.4	1.25	−0.41	−0.7
Concave-2	h: 0.6; r: 0.4	1.5	−0.43	−0.74
Concave-3	h: 0.5; r: 0.3	1.67	−0.34	−0.59
Concave-4	h: 0.7; r: 0.4	1.75	−0.46	−0.8
Concave-5	h: 0.5; r: 0.2	2.5	−0.29	−0.52

4 Results and Discussion

As mentioned before, we changed the physical parameters of the micro-/nanolenses on the substrate layer and designed different n-ZnO/NiO/p-GaN heterojunction-based white LEDs. We investigated the 3D distribution of DFT of E_y, 2D image map of DFT of E_y, EL intensity of light, light distribution, and EQE of the designed LEDs for performance analysis. Simulation results of the basic LED model and MNLA-based LEDs were compared. The impact of the physical parameters on the performance of the LEDs was analyzed for optimization.

4.1 *Performance of the Basic LED Without MNLA*

We investigated the EL light intensity and light distribution for the basic white LED of Figs. 3(a) and 3(d) at three observation points, namely, near field, far field 1, and far field 2. Figures 4(a)–4(c) illustrate the simulation results of the basic white LED model at the near field. The variation of EL intensity of E_y with the wavelength is illustrated in Fig. 4(a). At the near field, the highest EL intensity of 193,655 arbitrary units (a.u.) was detected at the wavelength of 645 nm. The 3D distribution of DFT of electric field component E_y is depicted in Fig. 4(b). The 2D image map of DFT of electric field component E_y at the near field is shown in Fig. 4(c). The simulation results of EL intensity of E_y, 3D distribution of DFT of E_y, and 2D image map of the basic white LED at the far field 1 are represented in Figs. 4(d), 4(e), and 4(f), respectively. At the far field 1, light distribution was smoother than the near field in the whole spectrum where the highest EL intensity of 27,835 a.u. was observed at the wavelength of 610 nm. The peak EL intensity at the far field 2 was detected at 580 nm, the value of which was 9760 a.u. [see Fig. 4(g)].

Spreading of light caused the decrease in peak EL intensity in the far field 1 and far field 2, compared to the near field, which is natural for incoherent light sources like LEDs. The 3D distribution of DFT and 2D image map of the basic LED at the far field 2 are shown in Figs. 4(h) and 4(i). The light intensity started to increase from the blue region (375 nm) and reached the peak in the green region and again started decreasing in the red region.

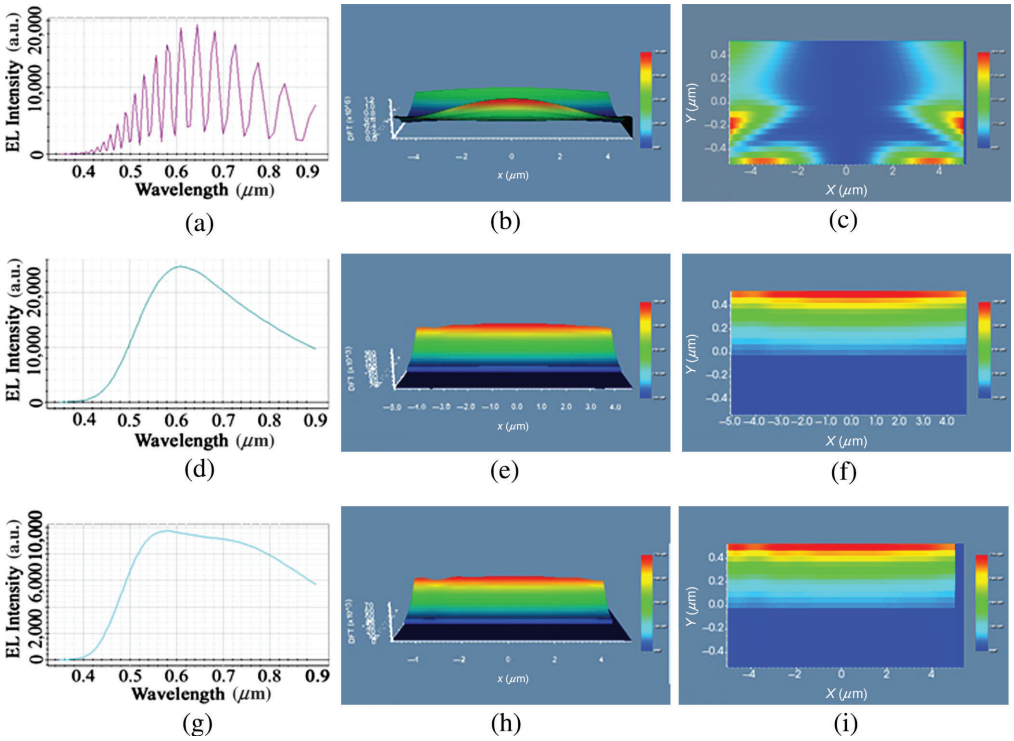

Fig. 4 Electric-field component of basic LED device without any micro-/nanostructure: (a)–(c) at the near field; (d)–(f) at the far field 1; and (g)–(i) at the far field 2: (a), (d), and (g) EL intensity of E_y; (b), (e), and (h) 3D distribution of DFT of E_y; and (c), (f), and (i) 2D image maps of DFT of E_y.

High-intensity light was detected throughout the visible spectrum (from 380 to 740 nm) that indicates the formation of white LED. The 3D distribution of DFTs and 2D image maps of electric field at different observation points signify consistent light output from the basic white LED. These results also confirmed excellent spreading of light with the increase of distance from the substrate layer of the LED.

4.2 *Performance of the Spherical MNLA Engraved LEDs*

To increase the out-coupling efficiency of the LEDs, we incorporated spherical shape planoconvex and planoconcave MNLA. During designing the LEDs, an array of tightly spaced half circle lenses was incorporated on top of the substrate layer where no space existed between the lenses in both horizontal and vertical directions. The radius of the planoconvex and planoconcave spherical lenses was varied from 0.4 to 0.7 μm.

4.2.1 *Planoconvex spherical MNLA engraved LEDs*

We started our simulation with planoconvex spherical lens array incorporated LEDs with lens radius/height of 0.4 μm. In order to examine the 3D distribution of light coming out from the LED, we investigated the 3D distributions of DFT of E_y at the near field, far field 1, and far field 2 locations after the substrate of the LEDs, as illustrated in Figs. 5(a)–5(c).

Afterward, we increased the radius of the planoconvex lenses from 0.5 to 0.7 μm. The 3D distributions of DFT of E_y at the near field, far field 1, and far field 2 for the LEDs with lens radius of 0.5, 0.6, and 0.7 μm are represented in Figs. 5(d)–5(f), 5(g)–5(i), and 5(j)–5(l), respectively. After the far field 2, significant improvement on consistency of light distribution was observed, as depicted in Figs. 5(c), 5(f), 5(i), and 5(l). The 3D distribution of DFT analysis exemplifies that MNLA incorporated LED with lens radius of 0.5 and 0.6 μm showed better results among all spherical planoconvex MNLA incorporated LEDs, when consistency of light distribution is considered.

Lens type	HRR	Near field (0 μm)	Far field 1 (8 μm)	Far field 2 (13 μm)
Spherical (Radius: 0.4 μm)	1	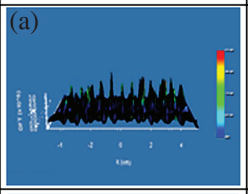	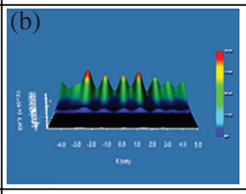	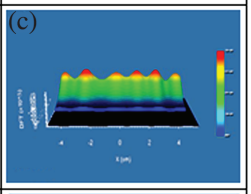
Spherical (Radius: 0.5 μm)	1	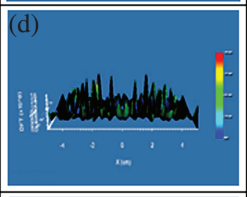	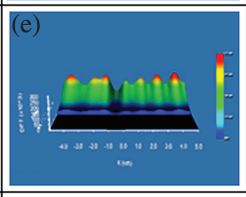	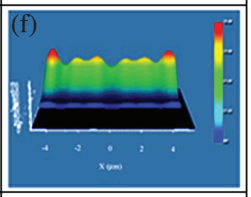
Spherical (Radius: 0.6 μm)	1	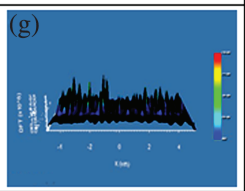	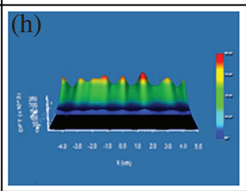	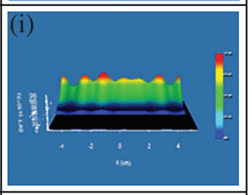
Spherical (Radius: 0.7 μm)	1	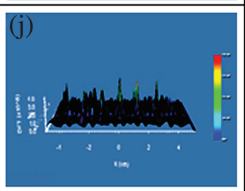	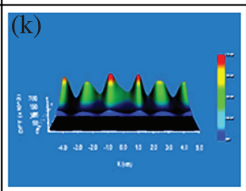	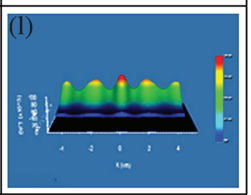

Fig. 5 3D distribution of DFT of E_y at (a), (d), (g), and (j): near field; (b), (e), (h), and (k): far field 1; and (c), (f), (i), and (l): far field 2 of the planoconvex spherical MNLA incorporated LEDs with lens radius varying from 0.4 to 0.7 μm: (a)–(c) $r = 0.4$ μm; (d)–(f) $r = 0.5$ μm; (g)–(i) $r = 0.6$ μm; and (j)–(l) $r = 0.7$ μm.

Figure 6 shows the 2D image map of DFT of E_y at the near field, far field 1, and far field 2 for all kinds of planoconvex spherical MNLA engraved LEDs. Because of the convex lenses at the end face of the substrate layer, light coming out from the LEDs was started focusing at the focal point of the lenses after the near field, as shown in Figs. 6(a), 6(d), 6(g), and 6(j).

After the focal point of the lenses, the light started to defocus and consequently, smooth light distribution was detected after the far field 1, especially for lens radius of 0.5 to 0.7 μm [see Figs. 6(e), 6(h), and 6(k)]. On the contrary, low spreading of light was observed in the far field 1 for lens radius of 0.4 μm, which is obvious from Fig. 6(b). In all cases, significant light spreading was detected in the far field 2 regions, as shown in Figs. 6(c), 6(f), 6(i), and 6(l). Compared to other MNLA engraved LEDs, the MNLA-based LEDs with lens radius of 0.5 and 0.6 μm showed better consistency in light distribution at the wave front after the far field 2, which is evident from Figs. 6(f) and 6(i). These results agree with the 3D distribution of DFT shown in Figs. 5(f) and 5(i).

Figure 7 illustrates the EL intensity of E_y at the far field 2 for the planoconvex spherical MNLA incorporated LEDs with lens radius varying from 0.4 to 0.7 μm. For 0.4 μm lens engraved LED, the peak EL intensity of light at the far field 2 was 13,100 a.u., which was observed at 524 nm [Fig. 7(a)]. Figure 7(b) represents the EL light intensity of E_y at the far field 2 for the planoconvex spherical MNLA incorporated LED having lens radius of 0.5 μm where the peak EL intensity of 14,240 a.u. was noticed at 584 nm. The peak EL intensity of E_y at the far field 2 for the 0.6-μm lens array incorporated LED was detected at 716 nm, the value of which was 14,655 a.u. [Fig. 7(c)]. For planoconvex 0.7 μm spherical lens engraved LED, the peak EL intensity of E_y at the far field 2 was 14,685 a.u. observed at 679 nm [Fig. 7(d)]. Significant amount of light was obvious in the visible spectrum indicating the formation of white LEDs. The EL intensity showed increasing trend with the increase of the lens radius where

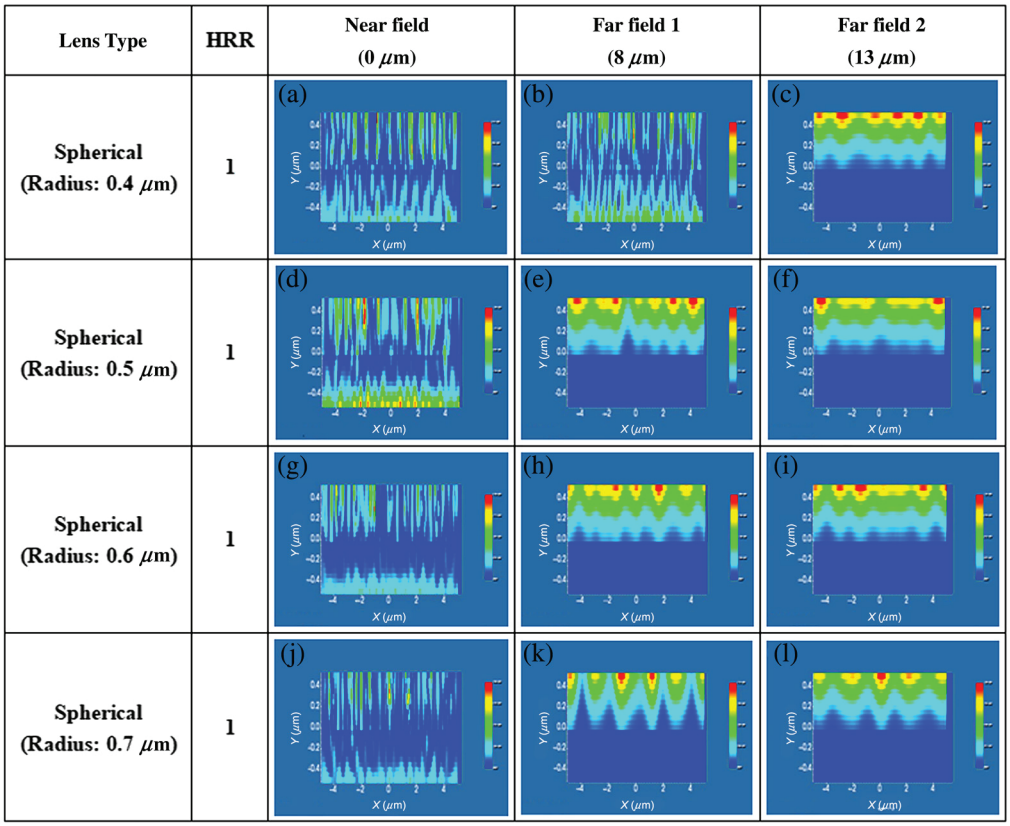

Fig. 6 2D image map of DFT of E_y at (a), (d), (g), and (j): near field; (b), (e), (h), and (k): far field 1; and (c), (f), (i), and (l): far field 2 of the planoconvex spherical MNLA incorporated LEDs with lens radius varying from 0.4 to 0.7 μm: (a)–(c) $r = 0.4$ μm; (d)–(f) $r = 0.5$ μm; (g)–(i) $r = 0.6$ μm; and (j)–(l) $r = 0.7$ μm.

highest EL intensity was detected in the 0.7-μm lens incorporated LED, which was slightly higher than the 0.6-μm lens engraved LED. However, because of the consistency of light distribution at the front end of the 0.6-μm MNLA incorporated LED, this LED can be considered as the fittest candidate among the planoconvex spherical MNLA incorporated LEDs.

4.2.2 *Planoconcave spherical MNLA engraved LEDs*

The 3D distributions of DFT at the near field, far field 1, and far field 2 for the MNLA incorporated LEDs with lens radius of 0.4, 0.5, 0.6, and 0.7 μm are depicted in Figs. 8(a)–8(c), 8(d)–8(f), 8(g)–8(i), and 8(j)–8(l), respectively.

After the near field, inconsistent light distribution was observed for all kinds of planoconcave MNLA engraved LEDs where the light distribution was improved after far field 1. After far field 2, consistency of light distribution was evident for most of the LEDs, as obvious from Figs. 8(c), 8(f), and 8(i). Still, inconsistent light distribution was evident for the MNLA-based LED with lens radius of 0.7 μm, as depicted in Fig. 8(l).

In order to investigate the light propagation at different locations after the substrate, we also studied the 2D image map of DFT of E_y at the near field, far field 1, and far field 2 for the planoconcave spherical MNLA incorporated LEDs (see Fig. 9). Because of the concave nature of the lenses, the light coming out from the planoconcave spherical MNLA incorporated LEDs started spreading immediately after the substrate layer where the results were verified by the images of Figs. 9(a), 9(d), 9(g), and 9(j). The simulation results confirmed more light spreading after far field 1 [Figs. 9(b), 9(e), 9(h), and 9(k)] and far field 2 [Figs. 9(c), 9(f), 9(i), and 9(l)] than the light spreading after the near field. In all cases, planoconcave spherical MNLA containing LEDs represented higher light spreading compared to the planoconvex spherical MNLA

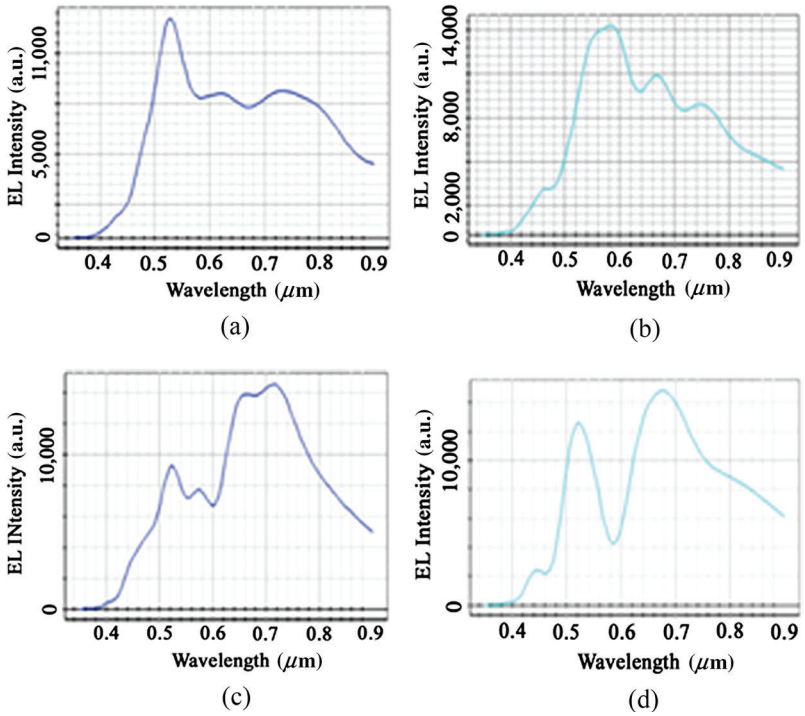

Fig. 7 EL intensity of E_y at far field 2 of the planoconvex spherical MNLA incorporated LEDs with lens radius varying from 0.4 to 0.7 μm: (a) $r = 0.4$ μm, (b) $r = 0.5$ μm, (c) $r = 0.6$ μm, and (d) $r = 0.7$ μm.

Lens type	HRR	Near field (0 μm)	Far field 1 (8 μm)	Far field 2 (13 μm)
Spherical (Radius: 0.4 μm)	1	(a)	(b)	(c)
Spherical (Radius: 0.5 μm)	1	(d)	(e)	(f)
Spherical (Radius: 0.6 μm)	1	(g)	(h)	(i)
Spherical (Radius: 0.7 μm)	1	(j)	(k)	(l)

Fig. 8 3D distribution of DFT of E_y at (a), (d), (g), and (j) : near field; (b), (e), (h), and (k): far field 1; and (c), (f), (i), and (l): far field 2 of the planoconcave spherical MNLA incorporated LEDs with lens radius varying from 0.4 to 0.7 μm: (a)–(c) $r = 0.4$ μm; (d)–(f) $r = 0.5$ μm; (g)–(i) $r = 0.6$ μm; and (j)–(l) $r = 0.7$ μm.

Lens type	HRR	Near field (0 μm)	Far field 1 (8 μm)	Far field 2 (13 μm)
Spherical (Radius: 0.4 μm)	1	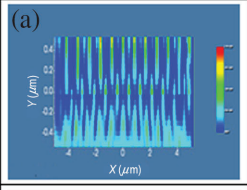	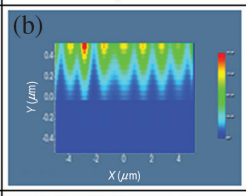	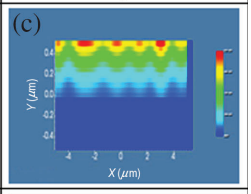
Spherical (Radius: 0.5 μm)	1	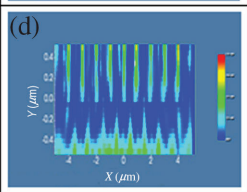	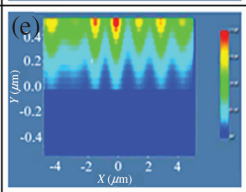	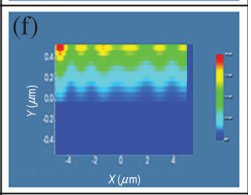
Spherical (Radius: 0.6 μm)	1	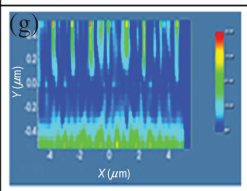	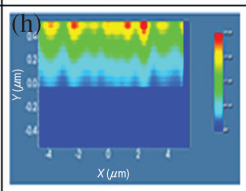	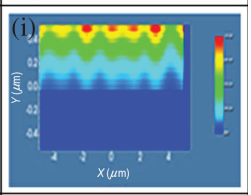
Spherical (Radius: 0.7 μm)	1	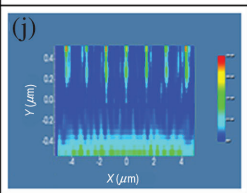	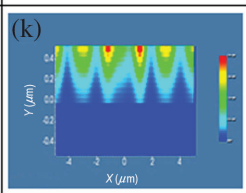	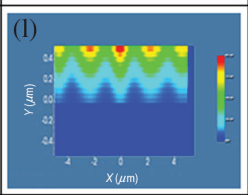

Fig. 9 2D image map of DFT of E_y at (a), (d), (g), and (j): near field; (b), (e), (h), and (k): far field 1; and (c), (f), (i), and (l): far field 2 of the planoconcave spherical MNLA incorporated LEDs with lens radius varying from 0.4 to 0.7 μm: (a)–(c) $r = 0.4$ μm; (d)–(f) $r = 0.5$ μm; (g)–(i) $r = 0.6$ μm; and (j)–(l) $r = 0.7$ μm.

containing LEDs. The 2D image maps at the far field 2 exemplify steady light distribution at the wave front when the lens radius was varying from 0.4 to 0.6 μm, which agreed with the 3D distribution of DFT shown in Fig. 8. Unfortunately, the MNLA-based LED with lens radius of 0.7 μm was inconsistent even after far field 2 and thus not suitable for commercial applications. Most of the planoconcave spherical MNLA incorporated LEDs showed improvement on light distribution, compared the planoconcave spherical MNLA-based LEDs.

The EL intensity of E_y at the far field 2 for the planoconcave spherical MNLA incorporated LEDs with lens radius varying from 0.4 to 0.7 μm was shown in Fig. 10. The existence of light all over the visible spectrum confirmed the development of white LEDs. For 0.4 μm lens containing LED, the peak EL intensity of light at the far field 2 was 10,320 a.u. detected at 510 nm, as evident from Fig. 10(a). This value is much lower than the peak EL intensity of light found in the planoconvex spherical MNLA incorporated LED with lens radius of 0.4 μm. Figure 10(b) shows the EL light intensity at the far field 2 for the planoconcave spherical MNLA engraved LED with lens radius of 0.5 μm. The peak intensity of 12,740 a.u. was noticed at 600 nm, which was much lower than the LED consisting planoconvex MNLA with lens radius of 0.5 μm. The peak EL intensity of E_y at the far field 2 for the 0.6-μm lens array engraved LED was noticed at 660 nm, the value of which was 14,900 a.u. [see Fig. 10(c)]. The EL intensity of the LED having planoconcave spherical MNLA of 0.6 μm lens radius was slightly higher than the corresponding LED comprising planoconvex spherical MNLA. In contrast, the peak EL intensity of E_y at the far field 2 for the planoconcave 0.7 μm spherical lens engraved LED was 14,360 a.u. at 523 nm [Fig. 10(d)], which was slightly lower than the corresponding planoconvex spherical MNLA-based LED. Among the planoconcave spherical MNLA-based LEDs, highest peak EL intensity was observed when the lens radius was 0.6 μm. Furthermore, this LED showed consistent light

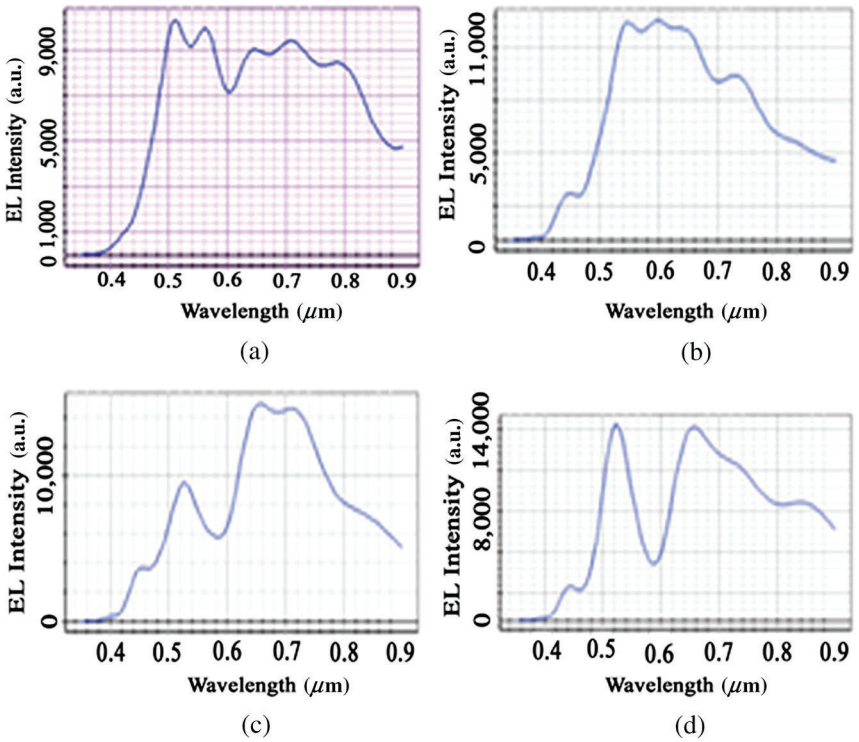

Fig. 10 EL intensity of E_y at far field 2 of the planoconcave spherical MNLA incorporated LEDs with lens radius varying from 0.4 to 0.7 μm: (a) $r = 0.4$ μm; (b) $r = 0.5$ μm; (c) $r = 0.6$ μm; and (d) $r = 0.7$ μm.

distribution at the wave front after far field 2 and thus can be considered as the best LED among the designed planoconcave spherical MNLA incorporated LEDs.

4.3 *Performance of the Elliptical MNLA Engraved LEDs*

We also studied the impact of aspherical, i.e., elliptical lenses on the performance of the LEDs. Both planoconvex and planoconcave MNLA were considered during the simulation where the MNLA were engraved at the end face of the substrate layer of the LEDs. The performance of the LEDs was evaluated using five different kinds of lenses, summarized in Table 2.

4.3.1 *Planoconvex elliptical MNLA engraved LEDs*

Our simulation started with planoconvex elliptical MNLA incorporated LED with convex-1 type lens with HRR of 1.25. Figures 11(a)–11(c) illustrate the 3D distribution of DFT of E_y at the near field, far field 1, and far field 2 for the convex-1 MNLA incorporated LED. The 3D distributions of DFT of E_y at the near field, far field 1, and far field 2 for the convex-2, convex-3, convex-4, and convex-5 type MNLA incorporated LEDs are shown in Figs. 11(d)–11(f), 11(g)–11(i), 11(j)–11(l), and 11(m)–11(n), respectively. Although distribution of light was inconsistent at the near field for all types of lenses, light distribution was improved significantly after far field 1 and far field 2. After far field 2, excellent intensity profile was evident for all kinds of planoconvex elliptical MNLA engraved LEDs where concave-1 structure showed best result.

Figure 12 showed the 2D image maps of DFT of E_y at the near field, far field 1, and far field 2 for all kinds of planoconvex elliptical MNLA incorporated LEDs indicating the light propagation pattern at different locations after the substrate. Since the lenses were convex, light was focused at the focal points of the lenses after the near field, as evident from the 2D image maps of Figs. 12(a), 12(d), 12(g), 12(j), and 12(m). After the focal points, the light started to defocus and consequently light spreading occurred. Light spreading continued even after far field 1 [Figs. 12(b), 12(e), 12(h), 12(k), and 12(n)] and far field 2 [Figs. 12(c), 12(f), 12(i), 12(l),

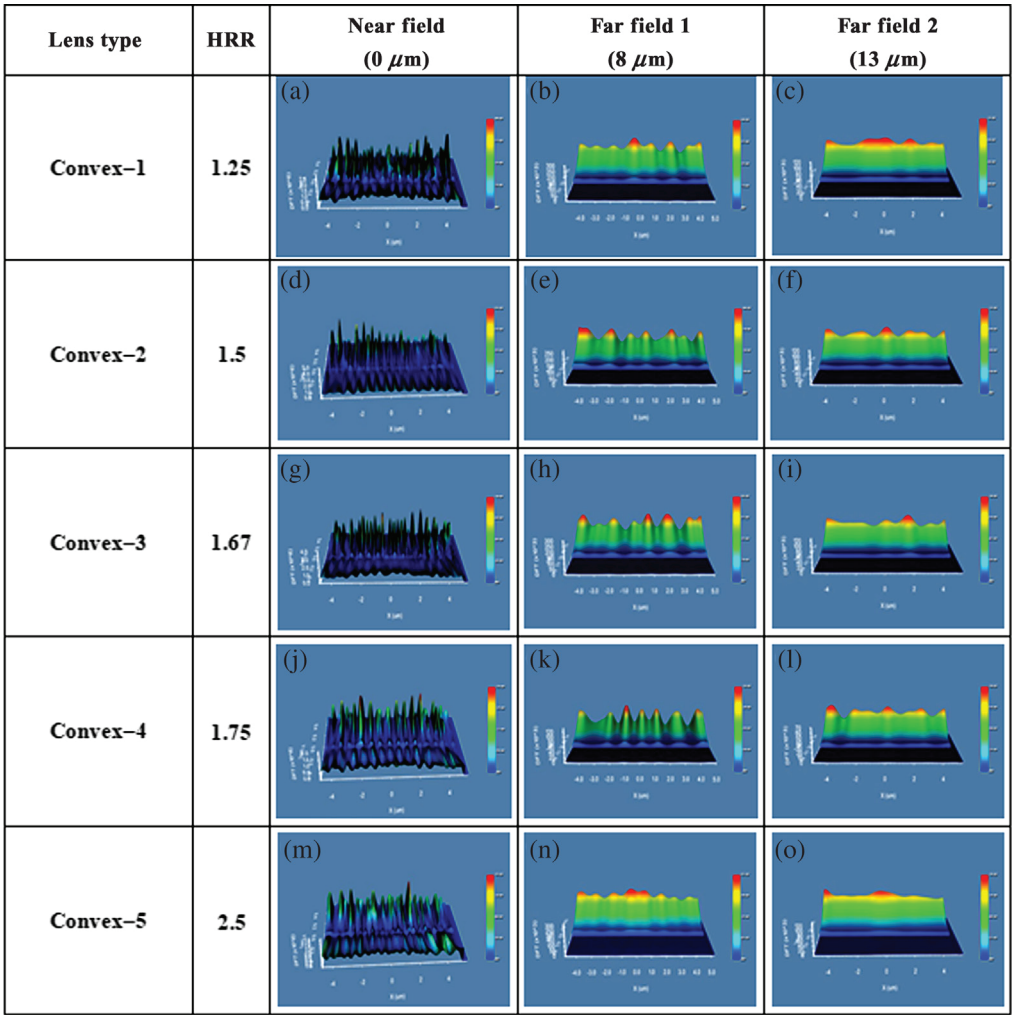

Fig. 11 3D distribution of DFT of E_y at (a), (d), (g), (j), and (m): near field; (b), (e), (h), (k), and (n): far field 1; and (c), (f), (i), (l), and (o): far field 2 of the planoconvex elliptical MNLA incorporated LEDs: (a)–(c) convex-1; (d)–(f) convex-2; (g)–(i) convex-3; (j)–(l) convex-4; and (m)–(o) convex-5.

and 12(o)]. The 2D image maps also confirmed consistent intensity profile for all kinds of planoconvex elliptical MNLA engraved LEDs, where convex-1 structure showed best result. Most importantly, significant improvement of light distribution was evident in the planoconvex elliptical MNLA-based LEDs, compared to the planoconvex spherical MNLA-based LEDs.

We also investigated the EL intensity of E_y at the far field 2 for the planoconvex elliptical MNLA incorporated LEDs, as shown in Fig. 13.

For all cases, significant light was evident throughout the visible spectrum indicating the formation of white LEDs. For convex-1 type elliptical lenses, the peak EL intensity of light at the far field 2 was 20,000 a.u. at the wavelength of 620 nm, as depicted from Fig. 13(a). The peak EL intensity of E_y at the far field 2 for the convex-2 type elliptical MNLA engraved LED was 16,600 a.u. at 630 nm, as illustrated in Fig. 13(b). For convex-3 elliptical lenses, the peak EL intensity of E_y at the far field 2 was detected at 626 nm where the value was 14,800 a.u., as shown in Fig. 13(c). The peak EL intensity of E_y at the far field 2 for the convex-4 type MNLA engraved LED was 14,300 a.u. that was noticed at 684 nm [see Fig. 13(d)]. The peak EL intensity of E_y at the far field 2 for the convex-5 type elliptical MNLA incorporated LED was significantly decreased, the value of which was 2000 a.u. at 620 nm [see Fig. 13(e)]. Except convex-5 type lenses, most of the planoconvex elliptical structures (convex-2 to convex-5) showed higher EL intensity, compared to all kinds of spherical structures (both planoconvex and planoconcave). Among the planoconvex elliptical structures, convex-1 type MNLA incorporated LED

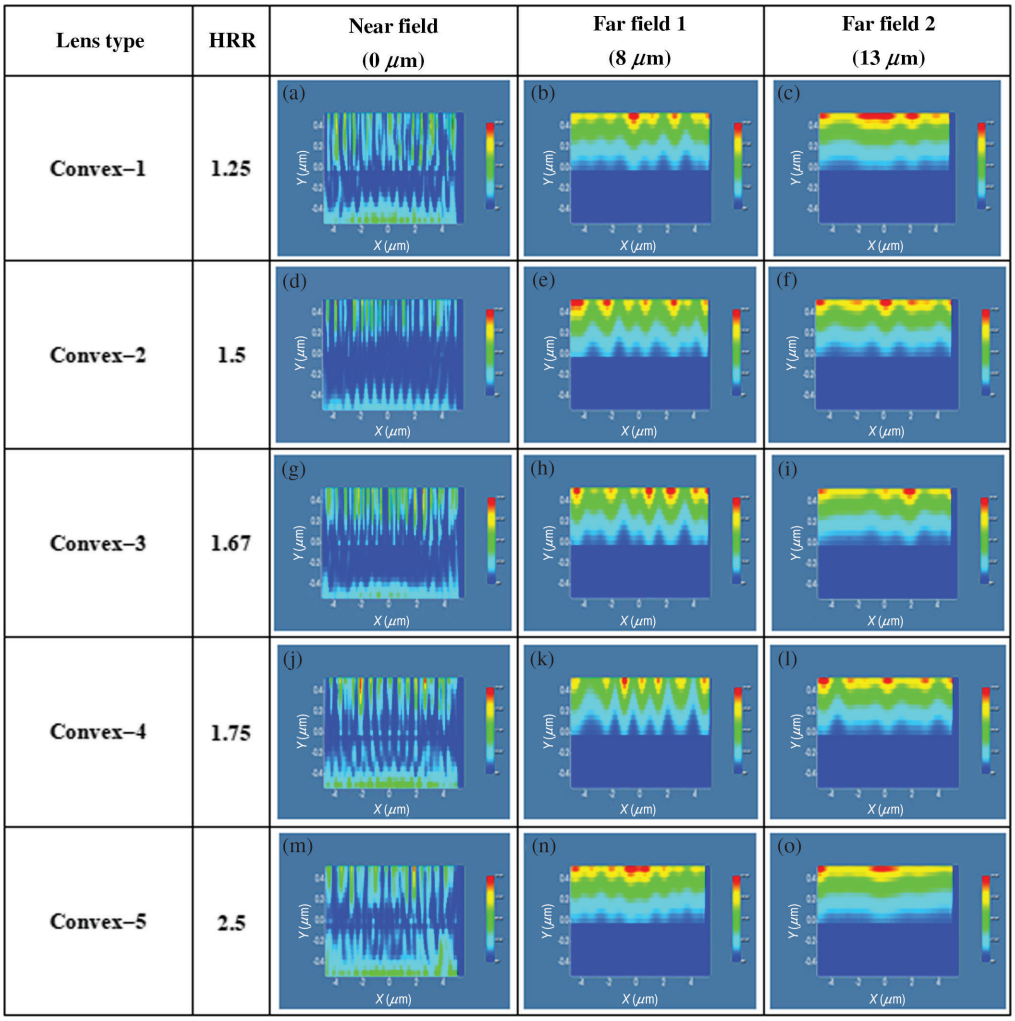

Fig. 12 2D image map of DFT of E_y at (a), (d), (g), (j), and (m): near field; (b), (e), (h), (k), and (n): far field 1; and (c), (f), (i), (l), and (o): far field 2 of the planoconvex elliptical MNLA incorporated LEDs: (a)–(c) convex-1; (d)–(f) convex-2; (g)–(i) convex-3; (j)–(l) convex-4; and (m)–(o) convex-5.

exhibited best performance in terms of EL light intensity along with consistent intensity profile, i.e., light distribution.

4.3.2 *Planoconcave elliptical MNLA engraved LEDs*

Like planoconvex elliptical MNLA incorporated LEDs, we investigated five different kinds of planoconcave elliptical MNLA incorporated LEDs (concave-1 to concave-5). Figure 14 shows the 3D distribution of DFT of E_y at near field, far field 1, and far field 2 for the planoconcave elliptical MNLA incorporated LEDs. At the near field of the LEDs, we observed inconsistent light distribution, as represented in Figs. 14(a), 14(d), 14(g), 14(j), and 14(m). With the increase of distance from the substrate layer, excellent smoothness of light distribution was noticed, as evident from the 3D distribution of DFT of E_y at the far field 1 and far field 2. At the far field 1, concave-1, concave-2, concave-3, and concave-5 types MNLA-based LEDs showed consistent light dissemination, as illustrated in Figs. 14(b), 14(e), 14(h), and 14(n), respectively. Farther improvement in consistency of light distribution was evident after the far field 2 for the concave-1, concave-2, concave-3, and concave-5 types MNLA-based LEDs, as depicted in Figs. 14(c), 14(f), 14(i), and 14(o), respectively. Like far field 1, light spreading was little inconsistent for the concave-4 type MNLA engraved LED, which was obvious from the 3D distribution of DFT of E_y shown in Fig. 14(l).

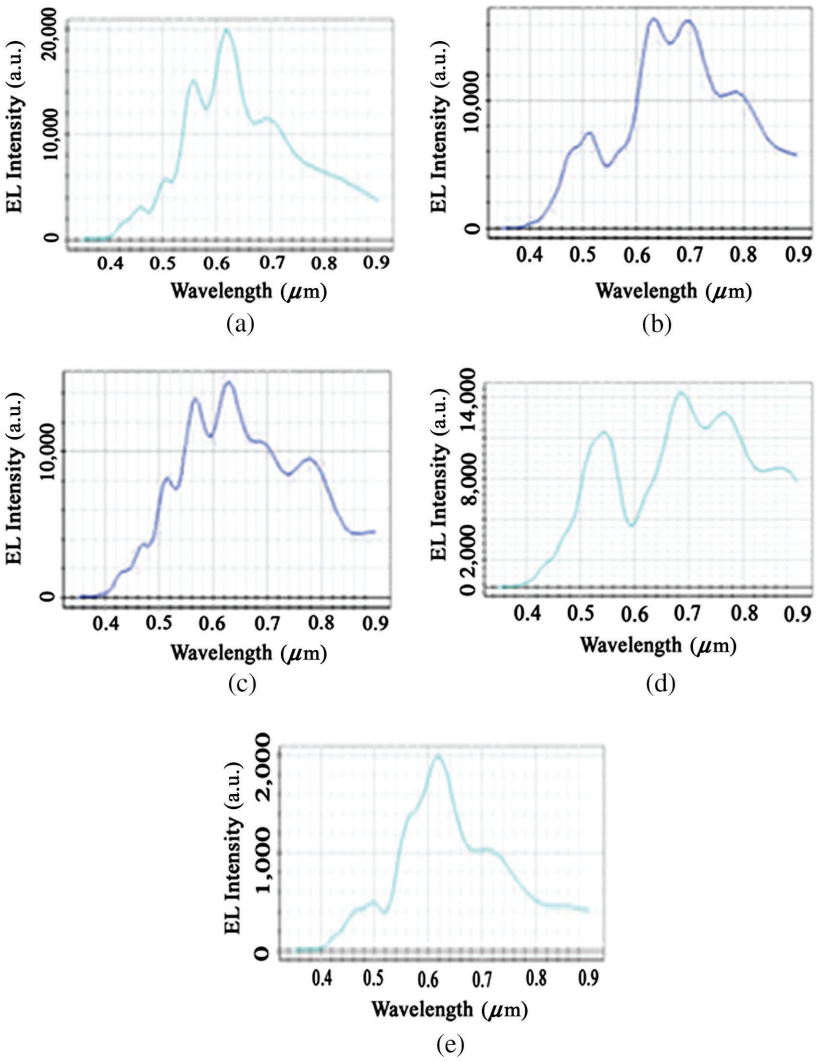

Fig. 13 EL intensity of E_y at far field 2 of the planoconvex elliptical MNLA incorporated LEDs: (a) convex-1; (b) convex-2; (c) convex-3; (d) convex-4; and (e) convex–5.

The light distribution of the planoconcave elliptical MNLA-based LEDs was also evident from the 2D image maps of DFT of E_y at the near field, far field 1, and far field 2 of Fig. 15.

Because of the concave type lenses, light started to spread immediately after the substrate layer, starting from the focal point of the lenses, which phenomenon was evident from the 2D image maps at the near field of the LEDs [Figs. 15(a), 15(d), 15(g), 15(j), and 15(m)]. From the 2D image maps at the far field 1, we can infer that concave-1, concave-2, concave-3, and concave-5 type MNLA engraved LEDs spread light consistently in all directions [as illustrated in Figs. 15(b), 15(e), 15(h), and 15(n)]. On the contrary, concave-4-based LED had inconsistent light distribution, as evident from Fig. 15(k). Similar kind of effect was observed in the 2D image maps at the far field 2. From light spreading point of view, concave-5 type MNLA engraved LED showed the best result among all kinds of planoconcave structures.

Figure 16 illustrates the EL light intensity of E_y for the planoconcave elliptical MNLA incorporated LEDs at the far field 2. The concave-1 MNLA engraved LED showed a peak EL light intensity of 15,300 a.u. at the wavelength of 604 nm [see Fig. 16(a)]. Figure 16(b) illustrates the EL light intensity at the far field 2 for concave-2 type MNLA-based LED where the peak EL intensity was 16,600 a.u. detected at 692 nm. Furthermore, we examined the EL intensity of E_y for the concave-3 type MNLA engraved LED at the far field 2, and the detected value of peak EL intensity of light was 14,600 a.u. at 640 nm, as illustrated in Fig. 16(c). The peak EL intensity of the concave-4 type MNLA-based LED was 11,600 a.u. at the wavelength of 742 nm

Lens type	HRR	Near field (0 μm)	Far field 1 (8 μm)	Far field 2 (13 μm)
Concave–1	1.25	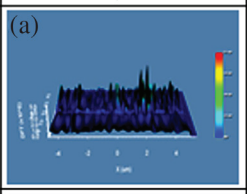 (a)	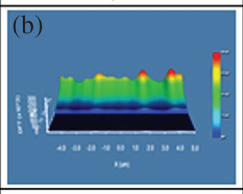 (b)	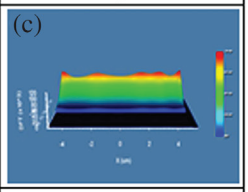 (c)
Concave–2	1.5	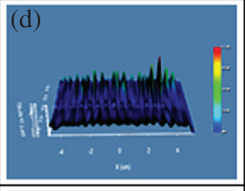 (d)	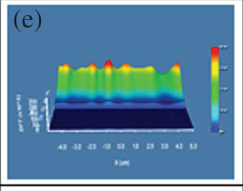 (e)	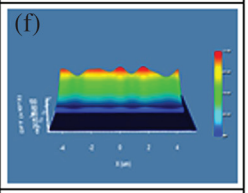 (f)
Concave–3	1.67	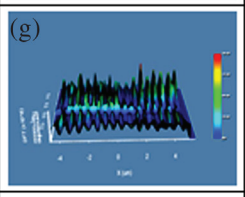 (g)	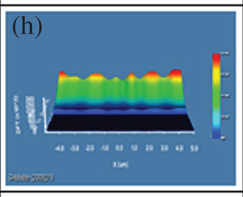 (h)	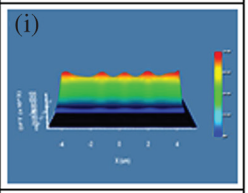 (i)
Concave–4	1.75	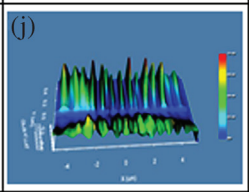 (j)	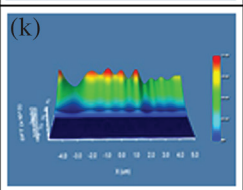 (k)	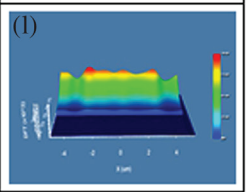 (l)
Concave–5	2.5	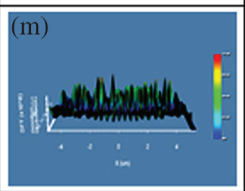 (m)	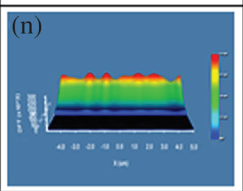 (n)	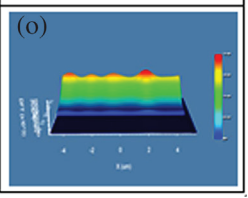 (o)

Fig. 14 3D distribution of DFT of E_y at (a), (d), (g), (j), and (m): near field; (b), (e), (h), (k), and (n): far field 1; and (c), (f), (i), (l), and (o): far field 2 of the planoconcave elliptical MNLA incorporated LEDs: (a)–(c) concave-1; (d)–(f) concave-2; (g)–(i) concave-3; (j)–(l) concave-4; and (m)–(o) concave-5.

[see Fig. 16(d)]. For convex-5 type MNLA engraved LED, the highest peak EL intensity of light at the far field 2 was detected at 604 nm, the value of which was 17,600 a.u., as shown in Fig. 16(e). Among all kinds of planoconcave elliptical MNLA engraved LEDs, concave-5 type MNLA engraved LED showed the highest EL light intensity with excellent light distribution.

4.4 *Impact of Physical Parameters of the MNLA on the Performance of LEDs*

There are two important parameters to evaluate the performance of an LED: EQE and intensity of light and their distribution. EQE has a direct relationship with the effective refractive index of the lens structures. We determined the effective refractive index for the best lens structures of different kinds (planoconvex spherical and elliptical and planoconcave spherical and elliptical) during the simulation. Using Eq. (3), we determined the EQE for the LEDs. EQE showed decreasing trend with the increase of effective refractive index. The basic LED structure showed an effective refractive index of 1.48. As a result, the EQE of the basic n-ZnO/NiO/p-GaN LED was 10.99%. For planoconvex spherical MNLA engraved LED with lens radius of 0.6 μm, the effective refractive index was 1.45. Consequently, we achieved an EQE of 11.49%. The effective refractive index of the planoconcave spherical MNLA-based LED structure was 1.44 and the

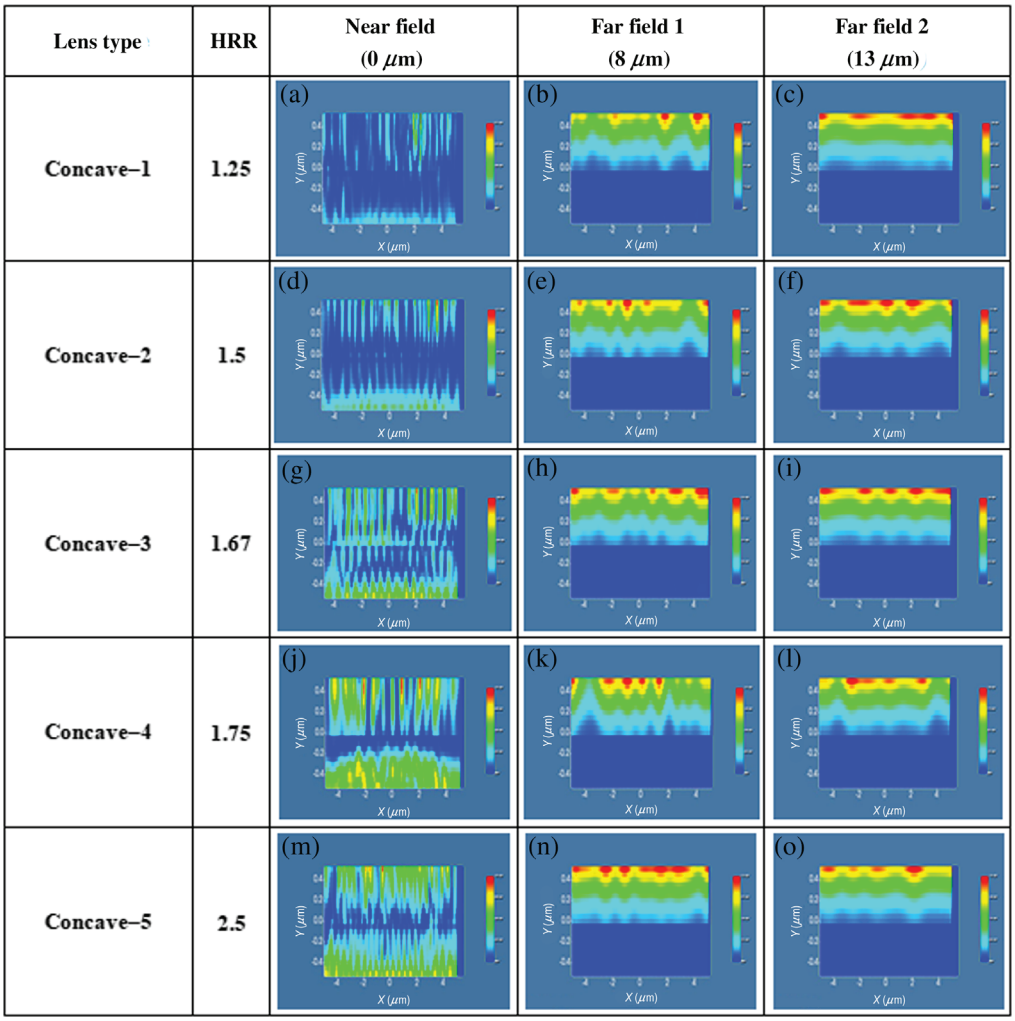

Fig. 15 2D image map of DFT of E_y at (a), (d), (g), (j), and (m): near field; (b), (e), (h), (k), and (n): far field 1; and (c), (f), (i), (l), and (o): far field 2 of the planoconcave elliptical MNLA incorporated LEDs: (a)–(c) concave-1; (d)–(f) concave-2; (g)–(i) concave-3; (j)–(l) concave-4; and (m)–(o) concave-5.

corresponding EQE was 11.66%. Elliptical lens engraved LEDs showed the better EQE compared to spherical lens engraved LEDs. We examined the effective refractive index of the concave-5 type elliptical MNLA engraved LED structure, the value of which was 1.42. As a consequence, the EQE was 12.02% for the concave-5 type planoconcave MNLA engraved LED structure. The effective refractive index of the convex-1 type elliptical MNLA incorporated LED structure was 1.4, which was lowest among all kinds of designed LEDs. Consequently, highest EQE of 12.4% was achieved for the convex-1 type planoconvex MNLA incorporated LED structure, which was 1.41% higher than the basic white LED.

As mentioned before, we studied the peak EL intensity of light for the basic LED and different MNLA engraved LEDs, where the highest peak EL intensity of light was observed in the convex-1 type elliptical MNLA-based LED structure. Table 3 summarizes the peak EL intensity of light at the far field 2 and EQE for the basic LED and the best MNLA structures of the four different kinds of micro-/nanometric structures along with their physical parameters. A closer look at the simulation results confirm that addition of light scattering structures, i.e., MNLA on the substrate layer improves the EL intensity of light in the visible spectrum and light extraction efficiency of the white LEDs. As a consequence, EQE of the MNLA engraved LEDs has improved significantly.

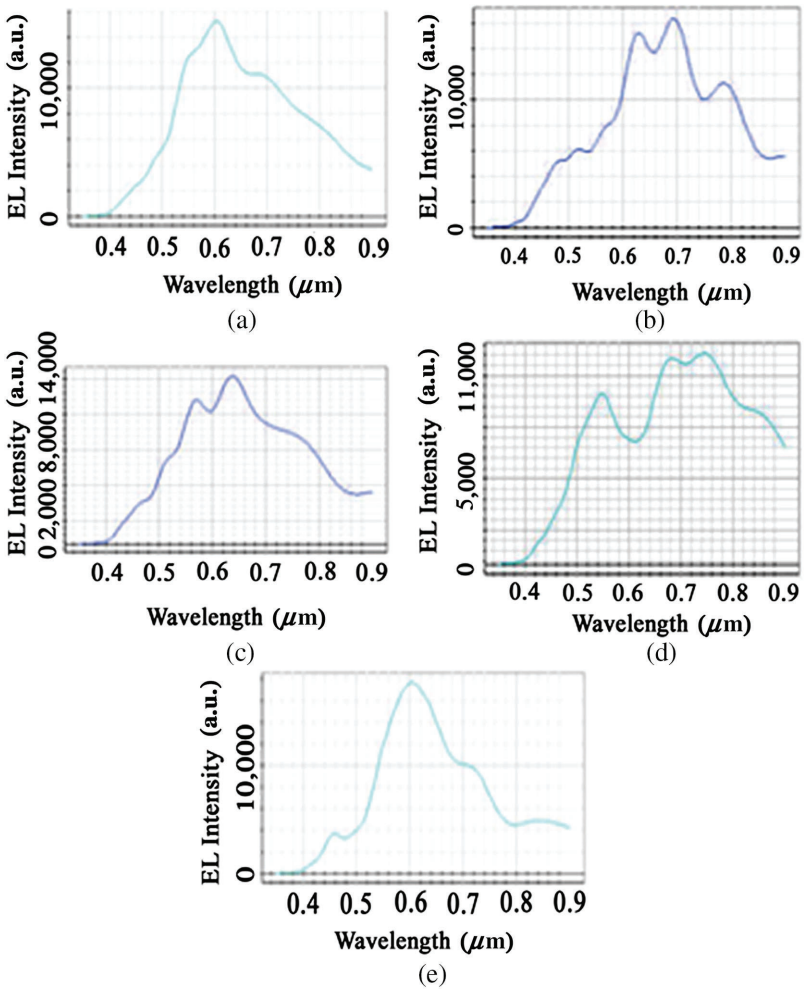

Fig. 16 EL intensity of E_y at far field 2 of the planoconcave elliptical MNLA incorporated LEDs: (a) concave-1; (b) concave-2; (c) concave-3; (d) concave-4; and (e) concave-5.

Table 3 Comparison of peak EL intensity of E_y at the far field 2 and EQE for different kinds of MNLA structured LEDs.

Structure type	Physical parameters (μm)	Peak EL intensity (a.u.)	EQE (%)
Basic structure (no additional structure)	Not applicable	9760 at 580 nm	10.99% for $n_e = 1.48$
Planoconvex spherical	r: 0.6 μm; HRR: 1	14,655 at 716 nm	11.49% for $n_e = 1.45$
Planoconcave spherical	r: 0.6 μm; HRR: 1	14,900 at 660 nm	11.66% for $n_e = 1.44$
Planoconvex elliptical (convex-1)	h: 0.5 μm; r: 0.4 μm; HRR: 1.25	20,000 at 620 nm	12.4% for $n_e = 1.4$
Planoconcave elliptical (concave-5)	h: 0.5 μm; r: 0.2 μm; HRR: 2.5	17,600 at 604 nm	12.02% for $n_e = 1.42$

However, all kinds of micro-/nanoscale lenses are not suitable for LED design because addition of some of the structures represent high degree of fluctuation in light distribution and light spreading. Thus proper selection of light scattering structure is important. As we know, light coming out from the closely located micro-/nanometric structures such as MNLA interfere with each other and create constructive pattern in some locations and destructive pattern in other

locations. The smoothness of light distribution depends on these patterns and the distance between the constructive/destructive patterns. The interference patterns change with the size, shape, and orientation of the MNLA. It is difficult to find a linear relationship between the physical parameters of the MNLA and the smoothness of light distribution. However, closely spaced constructive interference pattern definitely increases the smoothness of light distribution. From the simulation results, it is evident that elliptical MNLA structured LEDs have higher peak EL intensity of light compared to spherical MNLA structured LEDs. This phenomenon might have caused due to lens aberration effect, which is dominant in spherical lenses.[23] Among the spherical MNLA-based LEDs, when the radius of the lenses was 0.6 μm, the highest peak EL intensity with smooth light distribution was achieved in both planoconvex and planoconcave models. Thus 0.6 μm can be considered as the optimized radius for spherical lenses. In contrast, among the planoconvex elliptical MNLA-based LEDs, the highest peak EL intensity of light and consistent light distribution was detected for convex-1 structure (h: 0.5 μm and r: 0.4 μm) having lowest HRR (1.25) among the planoconvex MNLA structures. On the contrary, the highest peak EL intensity of light with smooth light spreading was observed for concave-5 structure (h: 0.5 μm and r: 0.2 μm) having the highest HRR (2.5) among the designed planoconcave MNLA structures, which was just opposite to the planoconvex elliptical models.

The efficiency of an LED can be increased by tailoring the light extraction efficiency. The outgoing light from the MNLA-based LEDs trapped inside the micro-/nanometric lenses of the substrate layer.[24,25] For a surface emitting LED, light is emitted from the substrate layer. Since the refractive index of the substrate layer is higher than the refractive index of air, some of the outgoing lights are reflected back from the substrate–air interface because of total internal reflection (TIR). The TIR can be reduced by modifying the physical structure of the substrate–air interface. Addition of micro-/nanometric structure on the substrate layer can change the critical angle required for TIR and thus increases the light extraction efficiency of the LED. Because of the curvature shape of the lenses, the incident angle of most of the lights was less than the critical angle and resisted TIR. Consequently, most of the outgoing light was refracted from the end face of the substrate layer for the MNLA engraved LEDs, rather than reflecting back inside the substrate layer (observed in flat surfaces, i.e., in basic LED). As a result, light extraction efficiency was increased, which in turn increased the EQE in the MNLA incorporated LEDs.

5 Conclusion

In summary, we achieved highly efficient white LEDs by incorporating MNLA on the substrate layer. The basic n-ZnO/NiO/p-GaN heterojunction-based LED showed an EQE of 10.99% with effective refractive index of 1.48. Addition of planoconvex and planoconcave MNLA structures on the substrate layer of the LED had increased the EQE and EL light intensity significantly. All kinds of the MNLA-based LEDs showed higher EQE and EL light intensity than the basic LED. Compared to spherical lenses, aspherical lenses showed higher light intensity at the output of the LEDs. However, some of these structures showed poor light distribution. To achieve high EQE accompanied by high-EL light intensity with smooth light distribution, we optimized the physical parameters of the micro-/nanolenses. Among spherical MNLA engraved LED models, planoconcave lens with lens radius of 0.6 μm showed the highest EQE of 11.66% at 660 nm with smooth light distribution. On the contrary, concave-5 MNLA, having the highest HRR (2.5), showed the highest EQE of 12.02% at 604 nm with excellent light distribution among planoconcave elliptical MNLA engraved LEDs. Simulation results confirmed convex-1 type MNLA-based LED, having lowest HRR (1.25), as the most promising structure showing a maximum EQE of 12.4% at 620 nm with effective refractive index of 1.4. The peak EL intensity of light of the convex-1 type MNLA incorporated white LED at the far field 2 was 20,000 a.u. at the wavelength of 620 nm, which was two times higher than the basic white LED. In addition to the highest EQE, this LED showed excellent light distribution and intensity profile in the visible spectrum. The proposed technique of efficiency and intensity enhancement can be considered as a potential tool for the development of highly efficient LEDs.

References

1. Y.-C. Lee and S.-H. Tu, *Recent Advances in Nanofabrication Techniques and Applications*, 1st ed., Intech, Rijeka (2011).
2. D. R. Opel et al., "Light-emitting diodes: a brief review and clinical experience," *J. Clin. Aesthet. Dermatol.* **8**(6), 36 (2015).
3. L. Riuttanen, "Diffusion injected light emitting diode," PhD Thesis, Aalto University, Finland (2015).
4. J. Hwang et al., "Development of InGaN-based red LED grown on (0001) polar surface," *Appl. Phys. Express* **7**(7), 071003 (2014).
5. R. H. Horng et al., "Fabrication and study on red light micro-LED displays," *IEEE J. Electron Devices Soc.* **6**, 1064 (2018).
6. K. Bukovinszky et al., "Green LED as an effective light source for curing acrylate-based dental resins in combination with Irgacure 784," *Adv. Cond. Matter Phys.* **2018**, 1 (2018).
7. P. Vashishtha et al., "High efficiency blue and green light-emitting diodes using Ruddlesden–Popper inorganic mixed halide perovskites with butylammonium interlayers," *Chem. Mater.* **31**(1) 83 (2019).
8. Y. Liu et al., "Efficient blue light-emitting diodes based on quantum-confined bromide perovskite nanostructures," *Nat. Photonics* **13**, 760 (2019).
9. Y. Jiang et al., "Spectra stable blue perobskite light emitting diodes," *Nat. Commun.* **10**, 1868 (2019).
10. X. L. Nguyen et al., "The fabrication of GaN-based light emitting diodes (LEDs)," *Adv. Nat. Sci.: Nanosci. Nanotechnol.* **1**, 025015 (2010).
11. L.-C. Chen et al., "Fabrication of GaN-based white light emitting diodes on yttrium aluminum garnet-polydimethylsiloxane flexible substrates," *Adv. Mater. Sci. Eng.* **2015**, 537163 (2015).
12. M. A. Abbasi et al., "The fabrication of white light-emitting diodes using the n-ZnO/NiO/p-GaN heterojunction with enhanced luminescence," *Nanosci. Res. Lett.* **8**, 320 (2013).
13. H.-K. Choi et al., "CO_2 laser assisted fabrication of micro-lensed single-mode optical fiber," *J. Opt. Soc. Korea* **19**(4), 327 (2015).
14. H.-K. Choi et al., "Formation of cylindrical micro-lens array on fused silica glass surface using CO2 laser assisted reshaping technique," *Opt. Laser Technol.* **75**, 63 (2015).
15. I.-B. Sohn et al., "Formation of a plano-convex micro-lens array in fused silica glass by using a CO2 laser-assisted reshaping technique," *J. Korean Phys. Soc.* **69**, 335 (2016).
16. I.-B. Sohn et al., "Laser assisted fabrication of micro-lens array and characterization of their beam shaping property," *Appl. Surf. Sci.* **479**, 375 (2019).
17. G. Keiser, *Optical Fiber Communications*, 2nd ed., McGraw-Hill Inc., Singapore (1991).
18. P. Anikeeva et al., "Electronic, optical and magnetic properties of materials," *Mater. Sci. Eng.* **3**, 24 (2013).
19. R. K. Garg, A. Dixit, and P. Yadav, *Basic Electronics*, 1st ed., Laxmi Publications (P) Ltd., Delhi (2008).
20. M. Polyanskiy, "Refractive index database," https://refractiveindex.info (accessed 14 June 2020).
21. M. S. Ahsan et al., "Efficiency improvement of organic light emitting diodes (OLEDs) using micro/nano-structures," in *Proc. ICEEICT* (2016).
22. R. Hasan et al., "Design and analysis of intense light beam by micro-lens engraved optical fiber," *Opt. Eng.* **58**(2) 027114 (2019).
23. R. S. Rafi, "Designing intense light beam by micro-structuring optical fiber," Masters Thesis, Khulna University, Bangladesh (2016).
24. N. I. Petrov et al., "Diffraction of partially-coherent light beams by microlens arrays," *Opt. Express* **25**(19), 22545 (2017).
25. P. Li et al., "Study on weak-light photovoltaic characteristics of solar cell with a micro-groove lens array on glass substrate," *Opt. Express* **23**(7), A192 (2015).

Apurba Adhikary received his BSc Engg and MSc Engg degrees in electronics and communication engineering from Khulna University, Khulna, Bangladesh. He has been serving as an assistant professor in the Information and Communication Engineering Department, Noakhali

Science and Technology University (NSTU), Noakhali, Bangladesh since January 2020. His research interests are currently focused on optical communication, optical soliton, and micro-/nanopatterning of various materials.

Md. Shamim Ahsan his BS degree in electronics and communication engineering from Khulna University, Bangladesh, in 2003 and his integrated MS/PhD in information and communications engineering from Korea Advanced Institute of Science and Technology (KAIST), Daejeon, Republic of Korea, in 2012. He currently holds the position of professor and head in Electronics and Communication Engineering Discipline, Khulna University, Bangladesh. His research interests are focused on laser processing of materials, passive optical networks, and nanophotonics.

Md. Mahbub Hossain received his BSc and MSc engineering degrees from Electronics and Communication Engineering Discipline, Khulna University, Khulna, Bangladesh, in 2003 and 2014, respectively. He is also a PhD fellow in the Department of Electrical and Electronic Engineering, Bangladesh University of Engineering and Technology, Dhaka, Bangladesh. Moreover, he is currently a faculty member at the Electronics and Communication Engineering Discipline, Khulna University, Bangladesh. His research interests are nanophotonics, plasmonics, optical biosensor, photonic crystal fiber, and wireless communication. He is also a reviewer of different Elsevier journals such as *Sensing and Biosensing Research* and *Optics Communication*.

Md. Bipul Hossain received his BSc and MSc degrees in information and communication engineering from Islamic University, Bangladesh. He is currently working as a lecturer of information and communication engineering at NSTU, Noakhali, Bangladesh. His current research interests are machine learning, computer vision, and optical communication.

S.H. Shah Newaz received his MSc and PhD degrees from KAIST, Daejeon, Republic of Korea, in 2010 and 2013, respectively. Currently, he is working as a lecturer at the Universiti Teknologi Brunei, Bandar Seri Begawan, Brunei and also holding an adjunct professor position at KAIST. He has written and co-authored in more than 60 prestigious international journals and conferences. He is a member of ACS and a senior member of IEEE.

Farid Ahmed received his BSc degree in electrical and electronic engineering from the University of Dhaka in 2003, his MSc degree in electrical engineering from Korea Advanced Institute of Science and Technology in 2007, and his PhD in mechanical engineering from the University of Victoria in 2015. Currently, he is an assistant professor at the University of Texas Rio Grande Valley. His research interest includes additive manufacturing, printed electronics, optical sensors, and laser material processing.

Ik-Bu Sohn received his BS and MS degrees from Inha University of South Korea and his PhD in 2003 from Kyungpook National University of South Korea, all in optical communications. He currently holds the position of principal research scientist at the Advanced Photonics Research Institute, Gwangju Institute of Science and Technology, Gwangju, Republic of Korea. His research interests are femtosecond laser micromachining of materials and its applications in the field of optical devices and nanophotonics.